ACS APPLIED MATERIALS & INTERFACES

Research Article

www.acsami.org

Layer-by-Layer Deposition of All-Nanoparticle Multilayers in Confined Geometries

Jonathan P. DeRocher,[†] Pan Mao,[‡] Jun Young Kim,[#] Jongyoon Han,[§,⊥] Michael F. Rubner,*[,#] and Robert E. Cohen*[,†]

[†]Department of Chemical Engineering, [‡]Department of Mechanical Engineering, [§]Department of Electrical Engineering and Computer Science, [⊥]Department of Biological Engineering, and [#]Department of Materials Science and Engineering, Massachusetts Institute of Technology, 77 Massachusetts Avenue, Cambridge, Massachusetts 02139, United States

ABSTRACT: Nanofluidic arrays containing high-aspect-ratio nanochannels were used as a platform for the deposition of all nanoparticle multilayers. LbL assembly of 6 nm titania and 15 nm silica nanoparticles resulted in conformal multilayers of uniform thickness throughout the nanochannels. These multilayers are inherently nanoporous with void volume fractions of about 0.5. Compared to unconfined assembly of the same materials on flat substrates, thinner multilayer films were observed for the case of deposition within confined channel geometries because of surface charge-induced electrostatic depletion of the depositing species. Additionally, systematic and reproducible bridging of the nanochannels occurred as multilayer assembly progressed, a phenomenon not seen in our earlier work involving polyelectrolytes. This behavior was attributed to relatively weak nanoparticle adsorption and the resulting formation of large aggregates. These results demonstrate a new route by which confined geometries can be coated and even bridged with a nanoporous multilayer without the need for calcination or other postassembly steps to introduce porosity into the conformal coating.

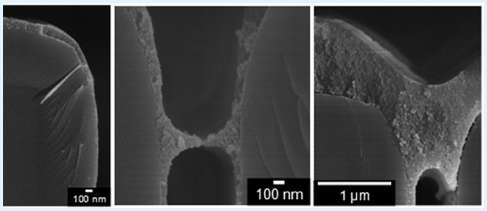

KEYWORDS: *layer-by-layer assembly, nanoparticle, nanochannel, confined geometry, directed assembly, nanofluidics*

The layer-by-layer assembly of polyelectrolytes in confined pores or channels has been studied extensively in recent years. Many researchers have used this flexible surface modification technique to manipulate the surface charge in microfluidic devices[1−3] or in thin capillaries used for electrophoresis,[4] to decorate confined surfaces with functional nanoparticles or biomolecules,[5] to enable stimuli-responsive gating,[6] and to tune the optical properties of photonic crystals.[7] Others have used LbL assembly within porous templates to form polymer nanotubes[8−11] and nanoporous polymer spheres.[12] Still others have focused on the fundamental behavior of polyelectrolyte deposition in confined geometries.[13−18] In earlier work, we have found that PAH/PSS multilayers assembled within confined geometries are thinner than those deposited on unconfined surfaces and that this effect is amplified by low ionic strength and by greater confinement.[16] Lazzara et al. came to very similar conclusions based on LbL deposition of dendrimers within the pores of AAO membranes.[17]

In a subsequent publication, we investigated the LbL assembly of two nanoparticle/polyelectrolyte pairs within confined nanochannels. We demonstrated that at low ionic strengths, drastically thinner multilayers are observed within confined channels, all without blocking or plugging of the channel itself. In this work, we extend these earlier results by investigating the LbL deposition of only nanoparticles within confined nanochannel arrays. In particular, we sequentially deposit silica and titania nanoparticles which have successfully been used to form antireflective, superhydrophilic, self-cleaning films[19] as well as a means of producing structural color[20−22] when deposited on flat surfaces. The use of only nanoparticles implies extra constraints on the assembly conditions due to their propensity for aggregation and their rigid nature.[23] Because of these added complications, the behavior of this nanoparticle system in nanochannels is of fundamental interest. Additionally, the ability to form an intrinsically nanoporous multilayer within a porous substrate without harsh post-treatments like calcination may be of practical value in applications such as selective separations.

EXPERIMENTAL SECTION

Materials. Titania nanoparticles (average particle size ∼6 nm) were synthesized by hydrolysis of titanium tetraisopropoxide as described in detail elsewhere.[24] Briefly, 2.5 mL of titanium tetraisopropoxide was dissolved in 50 mL of ethanol and added dropwise to an ice bath-cooled, continuously stirred solution of DI water which had been adjusted to pH 1.5 using nitric acid. The solution was stirred overnight on ice and then stored in a refrigerator. Silica nanoparticles (average particle size ∼15 nm) were purchased from Sigma-Aldrich (Ludox HS-40, 40 wt %). Nanochannel arrays were fabricated by thermal oxidation of approximately 1.5 μm silicon microchannels patterned by conventional photolithography as described in detail elsewhere.[25] The nanochannels were approximately 700 nm wide and 10 μm deep and therefore have an aspect ratio of

Received: October 23, 2011
Accepted: December 5, 2011
Published: December 19, 2011

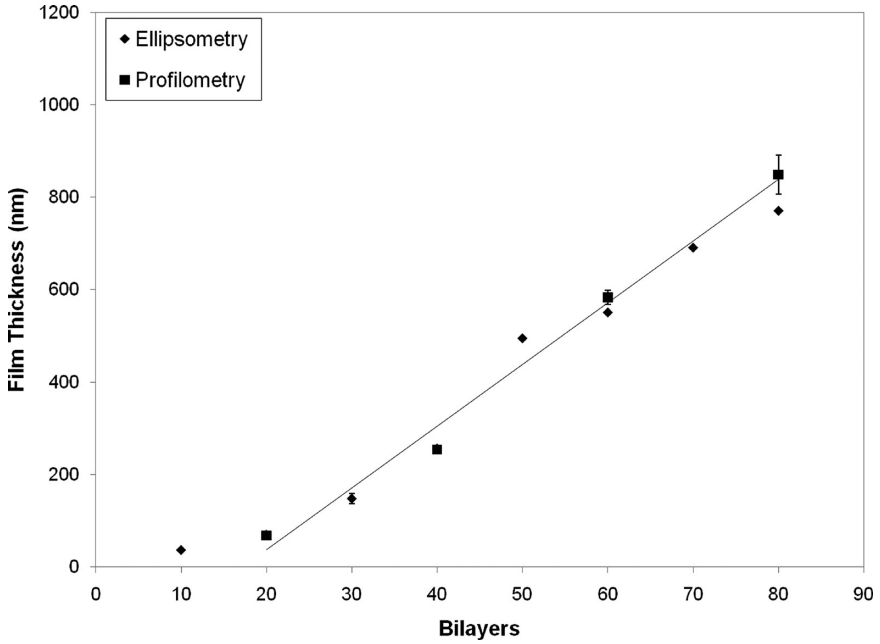

Figure 1. Nanoparticle multilayer thickness on planar silicon substrates as determined by ellipsometry (diamonds) and profilometry (squares). After an initial period of slow growth, the film grows linearly with a slope of about 13 nm/bilayer.

about 15. Silicon wafers were purchased from WaferNet Inc. and served as control planar substrates.

LbL Assembly. DI water (18.2 MΩ cm, Millipore Milli-Q) was used in all deposition solutions and rinse baths. The titania colloidal suspension was filtered using a 0.02 μm syringe filter (Anotop 25, Whatman) and diluted to 0.015 wt % with DI water adjusted to pH 1.5 using nitric acid. This silica suspension was filtered using a 0.2 μm syringe filter (Anotop 25, Whatman) and diluted to 0.015 wt % with pH 3.0 DI water. Rinse baths of the same pH as the deposition solution were prepared using DI water and filtered using 0.2 μm polyether sulfone filtration membranes (VWR). The titania rinse baths were adjusted using nitric acid to pH 1.5 while the silica rinse baths were adjusted to pH 3.0 with HCl.

Nanochannel array samples of approximately 0.5 cm^2 were affixed to glass slides using plasma-activated PDMS. These substrates as well as silicon wafer control samples were degreased by 10 min sonication in detergent solution (3% Micro-90, International Products Corp.) and then cleaned by 10 min sonication in 1 M HCl and in DI water. Automated LbL assembly was performed using a StratoSequence VI spin dipper (nanoStrata Inc.). Substrates were immersed in the titania and silica deposition suspensions for 15 min followed by three intermediate rinsing steps of 2, 2, and 1 min. The substrates were spun at 120 rpm during all deposition and rinsing steps. Every twenty bilayers, the deposition suspensions and rinse solutions were exchanged for fresh ones. Upon completion of LbL assembly, samples were removed immediately and dried with compressed air. These conditions and procedures mimic those used in our earlier work[26] on polymer/nanoparticle multilayers and are consistent with studies of nanoparticle LbL assembly on planar substrates.[19,20,23]

Characterization. The thicknesses of LbL-assembled nanoparticle films on planar silicon substrates were measured using spectroscopic ellipsometry (XLS-100, J.A. Woollam Co., Inc.) and profilometry (P-16+, KLA-Tencor). Films assembled within nanochannel arrays were characterized using SEM (JEOL 6320). Cross sectional samples were prepared by fracture of the coated array using a diamond scorer and sputter-coating with gold/palladium.

RESULTS AND DISCUSSION

Nanoparticle LbL assembly has been shown to occur only over a relatively small range of pH conditions.[23] This behavior is due to problems with nanoparticle suspension stability and the need for the zeta potentials of the two nanoparticle types to be comparable in magnitude so that charge reversal can occur. Without this careful balancing, layers significantly thinner than the nanoparticle diameter are deposited with each step, indicating partial coverage due to incomplete charge reversal. Lee et al.[23] undertook a detailed study of these effects for deposition of titania and silica particles and found that the bilayer thickness was especially sensitive to the pH of the silica nanoparticle suspension. In, particular, significant growth was only possible over a narrow pH range from 3 to 4. On the other hand, titania nanoparticles were prone to aggregation above pH 4, leading to opaque films. These results informed our selection of processing conditions for these experiments.

LbL assembly was carried out using pH 1.5 suspensions of positively charged titania nanoparticles and pH 3.0 suspensions of negatively charged silica nanoparticles. The thicknesses of all-nanoparticle films on planar silicon substrates were measured using ellipsometry and profilometry and are plotted in Figure 1. These data show robust multilayer growth with a bilayer thickness of about 13 nm. The negative intercept indicates that growth is patchy and uneven in the early stages of assembly and does not reach steady state until about 20 bilayers.

After confirming multilayer growth on planar substrates, LbL assembly of this all-nanoparticle system was attempted with nanochannel arrays. Cross-sectional SEM micrographs of fractured nanochannel array samples were taken to determine the structure of these nanoparticle multilayers within nanochannels. A set of wide view micrographs showing a large number of channels is given in Figure 2. These micrographs yield a number of interesting observations. First, it is clear that the channels are conformally and uniformly coated with nanoparticle multilayers with the exception of the channel entrance at high film thicknesses where bridging occurs. Second, it is clear that the unconfined tops of the posts exhibit significantly higher multilayer growth rates than the confined channels. Third, and most interestingly, we see systematic and reproducible bridging of the nanochannels around 40 bilayers

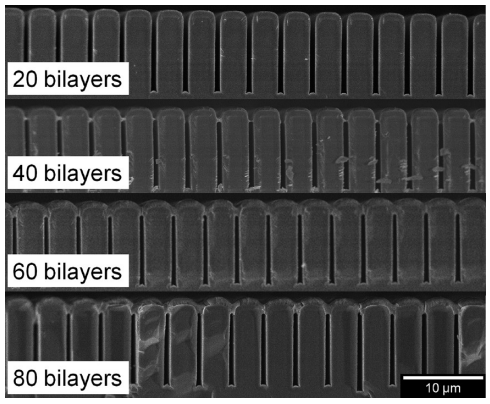

Figure 2. Composite micrograph highlighting the systematic nature of the bridging of nanochannels with TiO_2/SiO_2 nanoparticle multilayers. At 20 bilayers, no bridging is observed; after 40 bilayers, bridges begin to form; and at 60 and 80 bilayers, channels are completely covered.

and essentially complete covering of all nanochannels at 60 bilayers and above.

After 20 bilayers were deposited, we see results very similar to those observed previously for polymer/nanoparticle LbL deposition.[26] The multilayer conformally coats the entire channel uniformly and without any bridging or clogging. A magnified view of the nanochannel array subjected to 20 bilayers of LbL processing is presented in Figure 3. The

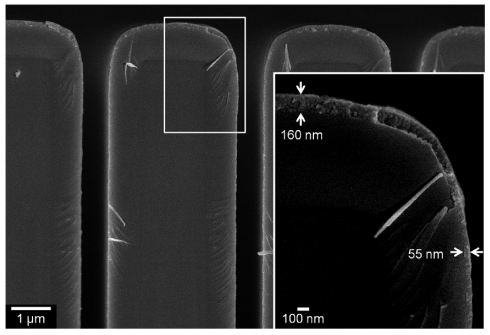

Figure 3. SEM micrograph of a nanochannel array coated with 20 bilayers of TiO_2/SiO_2 nanoparticles. Excellent conformality and uniformity are observed and the texture of the porous nanoparticle coating can be directly seen. The inset clearly shows the discrepancy between the thickness of the nanoparticle film on the top of the posts and that within the nanochannel.

production of the original channels involves a Si to SiO_2 oxidation step which leads to the observed 800 nm thick region visible just below the LbL coatings in all micrographs. Since the deposited multilayers are partly composed of silica, the contrast between the nanochannel substrate and the multilayer film is somewhat poor. Nevertheless, the texture difference between the nanoporous coating and the underlying substrate renders the film clearly visible. We can see that the thickness atop the posts is significantly larger than that within the channels.

After 40 bilayers were deposited, more complex assembly phenomena became noticeable. Figure 2 shows that at 40 bilayers about half of the nanochannels are completely bridged, some are completely open, and others show bridges in the process of forming. Figure 4 provides a magnified view of this substrate and provides a good example of all three of these

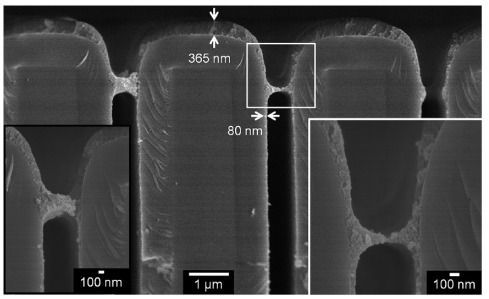

Figure 4. Micrograph of a nanochannel array coated with 40 bilayers of TiO_2/SiO_2 nanoparticles. Excellent conformality and uniformity are again observed, with the exception of bridge formation at the top of the channel. Examples of unbridged, newly bridged, and robustly bridged channels are shown. Significantly thicker multilayers are observed on the unconfined top of the posts compared with the confined walls of the channel. The insets provide magnified views of newly formed and thickened bridges.

states. The channel on the left is completely bridged, the one in the middle exhibits a very delicate bridge that has just been formed, and the one on the right is almost completely open, although we can observe a thickening of the film near the mouth of the channel where a bridge would eventually form. The insets show magnified views of fully formed and newly formed bridges. The discrepancy between unconfined and confined multilayer thicknesses is also more clearly evident at 40 bilayers. Although for some channels, this is attributable to blockage of the channel, other channels that have not been bridged still clearly exhibit this discrepancy.

After 60 bilayers of LbL processing, we obtain the structures seen in Figure 5 in which the thickness of the unconfined

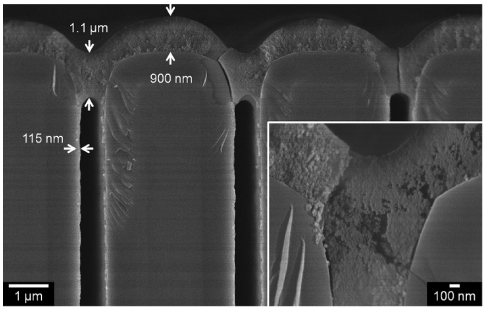

Figure 5. Micrograph of a nanochannel array subjected to 60 bilayers of TiO_2/SiO_2 nanoparticle deposition. Complete occlusion of the channel with a thick nanoporous multilayer is observed. Small defects near the channel openings are also evident, though many of these are likely caused by the fracture of the sample in preparation for imaging. The inset provides a magnified view of a nanochannel completely blocked by the nanoporous multilayer.

multilayer is now very substantial and the thicknesses of the bridges have increased substantially. In fact, the thickness of the bridge is greater than that of the multilayer on top of the posts, suggesting that the film grows rapidly over a channel once it has been bridged. Some defects are also evident in Figure 5. In one case, slight delamination from the surface appears to have occurred. This is likely due to the stresses which occur in the substrate and coating during fracture in preparation for SEM imaging. The fact that many defect-free channel bridges are also observed lends credence to this explanation. The other prominent defect is a small crack running through the bridge

along the midline of the channel. This may also be caused by the force of fracturing the sample, but reveals that in some cases the bridges have at the least a weak spot and possibly even a small crack running through the middle of them. Nearly all observed defects fell into one of these two categories.

After 80 bilayers were deposited, similar results are observed as shown in Figure 6. The thickness of the multilayer capping

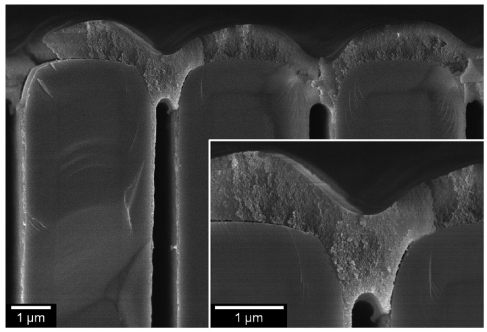

Figure 6. Micrograph of a nanochannel array subjected to 80 bilayers of TiO_2/SiO_2 nanoparticle deposition. The inset provides a magnified view of a nanochannel completely blocked by the nanoporous multilayer.

the entire substrate continues to grow and the thickness of the bridges remains higher than that of the unconfined multilayer. Although in general adhesion of the film is good, some small defects are present. Figure 7 provides a highly detailed view of

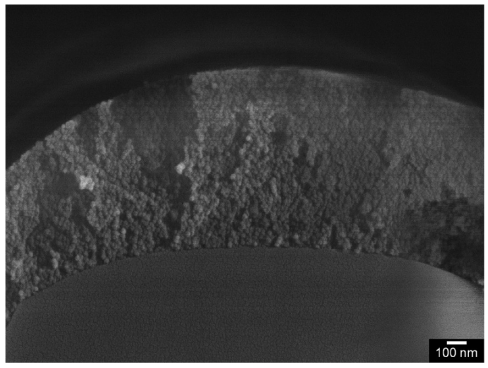

Figure 7. Highly magnified view of an 80 bilayer TiO_2/SiO_2 film deposited on a nanochannel array. The texture of the film and individual nanoparticles are clearly evident.

the multilayer itself. We can clearly see the texture inherent in this nanoporous coating and can even see individual nanoparticles which seem to be roughly close packed and appear to be consistent with the 15 nm diameter expected for SiO_2 nanoparticles.

Analysis of SEM images of coated nanochannel arrays was used to quantify our results and compare them with those obtained for planar substrates. This comparison is provided in Figure 8. The data for the exterior, or top of the nanochannels (triangles) show agreement with the trend observed using ellipsometry (diamonds) and profilometry (squares) on flat silicon wafers, but are systematically higher. Also significant are the large standard deviations associated with these SEM-based measurements as indicated by the error bars. Each of these points is the average of multiple measurements, indicating that although locally the film is very uniform, the variability across the substrate is relatively large. Comparison of the confined film thickness (circles) with the unconfined multilayer thickness and with the half channel width (dashed line) shows significantly slower growth within the channel and multilayers that remain much thinner than the theoretical maximum.

The deposition of nanoparticle multilayers before bridging occurs is consistent with the results for polymer/nanoparticle multilayers described elsewhere.[26] At low ionic strength, we once again observe significantly thicker multilayers on the unconfined top surfaces while the confined walls exhibit much slower growth. The multilayers are conformal and uniform at all depths within the channel, pointing to an equilibrium effect and not diffusion-limited transport of particles to the bottom of the channel. This is consistent with the idea of electrostatic exclusion of charged particles from the nanochannel because of the wall surface charge as laid out in detail in earlier publications.[16,17,26,27]

At around 40 bilayers, bridging begins to occur, deviating from the behavior observed previously for polymer/nanoparticle multilayers. One of the most interesting things about this phenomenon is the fact that bridging blocks every single nanochannel and tends to occur at exactly the same point at the mouth of each nanochannel. It seems clear that this bridging phenomenon is a general feature of all-nanoparticle multilayer deposition since similar experiments with polymer/nanoparticle multilayers consistently resulted in open nanochannels, even at high film thicknesses. This is likely due to the intrinsic properties of a charged nanoparticle. Unlike polymers, nanoparticles are rigid and therefore cannot bind simultaneously to many charged sites on the surfaces on which they deposit. As a result, nanoparticles are not adsorbed as strongly to the surface and desorb much more easily as a consequence. If a titania nanoparticle desorbs during the silica deposition step, it will bind with free silica particles in solution, forming a larger aggregate. The resulting aggregates have higher surface charge and are therefore even more strongly excluded from the confined nanochannel and may adsorb preferentially near the entrance.

The spinning of the substrate during deposition might also contribute to this phenomenon. Since the tops of the posts are directly exposed to the solution, adsorption of large aggregates might be less stable than within the nanochannel where the liquid is nearly stagnant. This would also explain the dramatically higher growth rate within the hollow above a newly formed bridge. Alternatively this higher growth in the notches above the bridges could be a simple consequence of the geometry; as the film grows from both sides of a V-shaped trench, the vertical depth of the film will grow more quickly than the thickness measured perpendicular to the sides of the trench.

Carillo and Dobrynin have recently performed molecular dynamics simulations of all-nanoparticle LbL assembly in confined geometries.[28] They simulated the deposition of five bilayers of oppositely charged nanoparticles on substrates containing cylindrical pores which were 2.5, 5, and 7.5 times larger than the nanoparticles being deposited. Taking the larger silica nanoparticles as a basis for comparison, these values correspond to 38, 65, and 113 nm pores in our system which are significantly smaller than the channels used here. Like us, they observed bridging of their pores, but at much lower film thicknesses because of their much smaller pores. They also found that slower growth occurs within the pores and that this growth plateaus as the pore becomes blocked. It is unclear from

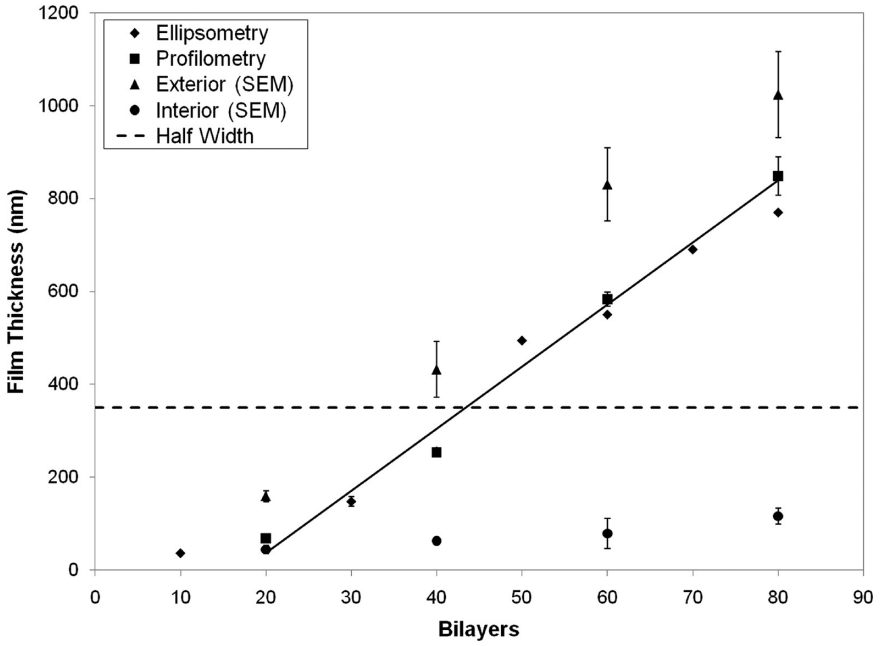

Figure 8. Thicknesses of TiO_2/SiO_2 multilayers deposited on planar silicon wafers and measured via ellipsometry and profilometry are compared with SEM measurements of multilayer thickness atop the posts (exterior) and on the walls of nanochannels (interior). The dashed line represents half the width of the nanochannel, the maximum film thickness achievable.

the fairly shallow pores they employed whether they, like us, see two distinct stages of growth within the pores: uniform, slow growth throughout the pore followed by bridging near the entrance of the pore. Their simulations do lead to a proposed mechanism for the bridging of the pores, suggesting that strings of positively charged and negatively charged nanoparticles form and that these aggregates bridge the pores. Their data show that nanoparticles desorb in pairs and that the resulting aggregates have more optimal electrostatic interactions than they had in the adsorbed state. This mechanism is qualitatively consistent with our results, showing that nanoparticles are particularly susceptible to desorption and that this results in aggregation and bridging of small pores or channels.

CONCLUSIONS

In this work, we have demonstrated that LbL deposition of titania and silica nanoparticles in confined geometries results in conformal and uniform coverage of the channels and then reproducible, systematic bridging of the channel mouths. Films deposited on the confined channel walls were significantly thinner than those assembled on the unconfined tops of the posts. This is in agreement with theoretical and experimental results which show that electrostatic exclusion of depositing species is important for LbL deposition in extreme confinement or at low ionic strength. The bridging of the nanochannels was attributed to the weak adsorption of nanoparticles and to the ease with which they desorb to form large aggregates. Significant variability in the unconfined film thickness over macroscopic distances was also observed, indicating that LbL deposition of nanoparticles is more sensitive to the local geometry than polymer/nanoparticle assembly.

This work provides a new route by which confined geometries can be coated with a nanoporous multilayer without the need for calcination. In addition, the systematic bridging of these channels is intriguing in that it results in the plugging of large nanochannels with a nanoporous layer. This unique geometry points to applications in selective separations wherein this porous layer could be deposited on an unselective, highly porous film. The thickness and functionality of the nanoparticle layer could be manipulated to provide high selectivity while preserving relatively high flux of the permeating species.

AUTHOR INFORMATION

Corresponding Author

*Telephone: 617-253-4477 (M.F.R.); 617-253-3777 (R.E.C.). Fax: 617-258-7874 (M.F.R.); 617-258-8224 (R.E.C.). E-mail: rubner@mit.edu. (M.F.R.); recohen@mit.edu (R.E.C.).

ACKNOWLEDGMENTS

This work was supported in part by the MRSEC Program of the National Science Foundation under award number DMR 0819762. The authors thank the MRSEC Shared Experimental Facilities and the Institute for Soldier Nanotechnologies (ISN) for use of characterization facilities and Mr. Hyomin Lee for assistance with profilometry measurements.

REFERENCES

(1) Barker, S. L. R.; Ross, D.; Tarlov, M. J.; Gaitan, M.; Locascio, L. E. *Anal. Chem.* **2000**, *72*, 5925−5929.
(2) Barker, S. L. R.; Tarlov, M. J.; Canavan, H.; Hickman, J. J.; Locascio, L. E. *Anal. Chem.* **2000**, *72*, 4899−4903.
(3) Sui, Z.; Schlenoff, J. B. *Langmuir* **2003**, *19*, 7829−7831.
(4) Graul, T. W.; Schlenoff, J. B. *Anal. Chem.* **1999**, *71*, 4007−4013.
(5) Liu, Y.; Xue, Y.; Ji, J.; Chen, X.; Kong, J.; Yang, P.; Girault, H. H.; Liu, B. *Mol. Cell. Proteomics* **2007**, *6*, 1428−1436.
(6) Lee, D.; Nolte, A. J.; Kunz, A. L.; Rubner, M. F.; Cohen, R. E. *J. Am. Chem. Soc.* **2006**, *128*, 8521−8529.
(7) Arsenault, A. C.; Halfyard, J.; Wang, Z.; Kitaev, V.; Ozin, G. A.; Manners, I.; Mihi, A.; Miguez, H. *Langmuir* **2005**, *21*, 499−503.
(8) Chia, K.-K.; Rubner, M. F.; Cohen, R. E. *Langmuir* **2009**, *25*, 14044−14052.
(9) Lee, D.; Cohen, R. E.; Rubner, M. F. *Langmuir* **2007**, *23*, 123−129.

(10) Ai, S.; Lu, G.; He, Q.; Li, J. *J. Am. Chem. Soc.* **2003**, *125*, 11140−11141.
(11) Hou, S.; Harrell, C. C.; Trofin, L.; Kohli, P.; Martin, C. R. *J. Am. Chem. Soc.* **2004**, *126*, 5674−5675.
(12) Wang, Y.; Caruso, F. *Chem. Mater.* **2006**, *18*, 4089−4100.
(13) Wang, Y.; Angelatos, A. S.; Dunstan, D. E.; Caruso, F. *Macromolecules* **2007**, *40*, 7594−7600.
(14) Angelatos, A. S.; Wang, Y.; Caruso, F. *Langmuir* **2008**, *24*, 4224−4230.
(15) Alem, H.; Blondeau, F.; Glinel, K.; Demoustier-Champagne, S.; Jonas, A. M. *Macromolecules* **2007**, *40*, 3366−3372.
(16) DeRocher, J. P.; Mao, P.; Han, J.; Rubner, M. F.; Cohen, R. E. *Macromolecules* **2010**, *43*, 2430−2437.
(17) Lazzara, T. D.; Lau, K. H. A.; Abou-Kandil, A. I.; Caminade, A.-M.; Majoral, J.-P.; Knoll, W. *ACS Nano* **2010**, *4*, 3909−3920.
(18) Roy, C. J.; Dupont-Gillain, C.; Demoustier-Champagne, S.; Jonas, A. M.; Landoulsi, J. *Langmuir* **2009**, *26*, 3350−3355.
(19) Lee, D.; Rubner, M. F.; Cohen, R. E. *Nano Lett.* **2006**, *6*, 2305−2312.
(20) Wu, Z.; Lee, D.; Rubner, M. F.; Cohen, R. E. *Small* **2007**, *3*, 1445−1451.
(21) Kurt, P.; Banerjee, D.; Cohen, R. E.; Rubner, M. F. *J. Mater. Chem.* **2009**, *19*, 8920−8927.
(22) Nogueira, G. M.; Banerjee, D.; Cohen, R. E.; Rubner, M. F. *Langmuir* **2011**, *27*, 7860−7867.
(23) Lee, D.; Omolade, D.; Cohen, R. E.; Rubner, M. F. *Chem. Mater.* **2007**, *19*, 1427−1433.
(24) Choi, W.; Termin, A.; Hoffmann, M. R. *J. Phys. Chem.* **1994**, *98*, 13669−13679.
(25) Mao, P.; Han, J. *Lab Chip* **2009**, *9*, 586−591.
(26) Kim, J. Y.; DeRocher, J. P.; Mao, P.; Han, J.; Cohen, R. E.; Rubner, M. F. *Chem. Mater.* **2010**, *22*, 6409−6415.
(27) Böhmer, M. R.; Evers, O. A.; Scheutjens, J. M. H. M. *Macromolecules* **1990**, *23*, 2288−2301.
(28) Carrillo, J.-M. Y.; Dobrynin, A. V. *ACS Nano* **2011**, *5*, 3010−3019.